



La(Sr)Ga(Fe)O₃ Perovskite Oxide as a New Mixed Ionic-Electronic Conductor for Oxygen Permeating Membrane

Tatsumi Ishihara,^{*,z} Yuko Tsuruta, Yu Chunying, Toshitsune Todaka, Hiroyasu Nishiguchi, and Yusaku Takita

Department of Applied Chemistry, Faculty of Engineering, Oita University, Dannoharu 700, Oita 870-1192, Japan

Fe-doped La_{1-x}Sr_xGaO₃ exhibits a high conductivity (~1 S/cm) and a high oxygen permeation rate. In particular, the highest conductivity and the oxygen permeating rate were attained at La_{0.7}Sr_{0.3}Ga_{0.6}Fe_{0.4}O₃ (LSGF). Although a surface catalyst is required, oxygen permeation rate from air to Ar was as high as 2.5 cm³ std/min cm² at 1273 K and 0.3 mm membrane thickness. Oxygen permeation rate from air to Ar increased in the following order, La_{0.6}Sr_{0.4}CoO₃ > La_{0.9}Sr_{0.1}CoO₃ = Sm_{0.5}Sr_{0.5}CoO₃ ≫ Sm_{0.6}Sr_{0.4}CoO₃, as the surface catalyst. Since the p_{O₂} gradient becomes larger, the oxygen permeation rate drastically increased by changing from air-Ar to CH₄-air condition. The products were only CO and H₂, having a molar ratio (H₂/CO ratio) of almost two. Electronic hole conduction was only observed in LSGF polarization measurement and the oxide ion conductivity estimated is as high as $s = 0.6 \text{ S cm}^{-1}$ at 1073 K. At high p_{O₂}, the main defect in LSGF is O_i' and Fe_{Fe}[•], and at intermediate p_{O₂}, concentration of Fe_{Fe}[•] is balanced with that of O_i'. The estimated transport number of oxide ion was ca. 0.6, which is in a good agreement with that estimated by the electromotive force in H₂-O₂ gas concentration cells. © 2002 The Electrochemical Society. [DOI: 10.1149/1.1524174] All rights reserved.

Manuscript submitted January 22, 2002; revised manuscript received July 3, 2002. Available electronically November 21, 2002.

Methane (CH₄) is the major component in natural gas which is an abundant natural resource. Therefore, conversion of CH₄ into useful compounds is an important subject at present. From the viewpoint of the useful utilization of CH₄, the partial oxidation of CH₄ is attractive, because the reaction gives a synthesis gas at CO:H₂ = 1:2, which is suitable for the synthesis of methanol or hydrocarbons. Pure oxygen gas is an essential reactant for this reaction and as far as the cost is concerned, separation of air into O₂ and N₂ by a simple method should be considered. Separation of air into O₂ and N₂ by a mixed electronic and oxide ionic conducting ceramic membrane is an ideal method for obtaining pure oxygen because of its simple structure and low energy consumption.¹ However, separation of oxygen with mixed conducting membrane requires p_{O₂} gradient. Since p_{O₂} in CH₄ stream is smaller than 10⁻²⁰ atm, application of oxygen separation with mixed conducting ceramic membrane for CH₄ partial oxidation is an ideal application of the mixed conducting ceramic membranes.

It is well known that La(Sr)Fe(Co)O₃ (LSFC) perovskite oxides exhibit superior mixed conductivity and, consequently, a high oxygen permeation rate is attained on these perovskite oxides.² In particular, it is reported that SrCoO₃ doped with Ca and Fe for Sr and Co sites, respectively, exhibits an extremely high oxygen permeation rate.³ However, LSFC is easily reduced in CH₄ atmosphere and it is reported that failure of the membrane due to reduction sometimes occurs when LSFC is used as the oxygen-permeating membrane for CH₄ partial oxidation.⁴ It is reported that SrFeCo_{0.5}O₃ is stable against reduction and it can be used as the oxygen-permeating membrane for the partial oxidation of methane.^{5,6} However, synthesis of this oxide is rather difficult, and further improvement in the oxygen-permeating rate is required for the application of the mixed electronic-oxide ionic conductor to the oxygen generator for CH₄ partial oxidation.

In our previous study, it was found that Ni- or Fe-doped La(Sr)GaO₃ was a mixed electronic hole and oxide ionic conductor and the material was stable over a wide range of oxygen partial pressures (p_{O₂}).^{7,8} In particular, it was found that Fe-doped La(Sr)GaO₃ exhibited high electrical conductivity and an oxygen-permeating rate.⁹ Therefore, Fe-doped La(Sr)GaO₃ is expected as

the oxygen permeation membrane for CH₄ partial oxidation. In this study, therefore, mixed electronic and oxide ionic conductivity in Fe-doped La(Sr)GaO₃ was investigated in detail. Furthermore, oxygen-permeating properties through La(Sr)Ga(Fe)O₃ (LSGF) membrane under CH₄ partial oxidation were studied.

Experimental

Sample preparation.—Fe-doped La(Sr)GaO₃ was prepared by a conventional solid-state reaction using La₂O₃ (99.99%, Wako Pure Chemicals), SrCO₃ (reagent grade, Wako Pure Chemicals), Ga₂O₃ (99.99%, Kishida Chemicals), and Fe₂O₃ (99.5%, Wako Pure Chemicals). Metal oxides of the desired compositions were milled in an Al₂O₃ mortar and pestle and the mixture subsequently calcined at 1273 K for 6 h. The powder after calcination was mixed again and pressed into a disk (20 mm diam) followed by isostatic pressing at 2700 kg/cm² for 20 min. The obtained disks were sintered at 1773 K for 6 h. Finally, disks were ground to 0.5 mm thickness on a diamond wheel. It is also noted that change in the composition during preparation is not observed by inductively coupled plasma (ICP) measurement. In order to improve the surface activity for oxygen dissociation, each disk was painted on both surfaces with La(Sr)CoO₃ (denoted as LSC) or Sm(Sr)CoO₃ (SSC) slurry at 10 mm diam with a brush. La_{0.6}Sr_{0.4}CoO₃ was mainly used for this purpose. LSC or SSC was prepared by calcination of the mixture of reagent-grade La(NO₃)₃, Sm₂O₃, Sr(NO₃)₂, and (CH₃COO)₂Co (Kishida Chemicals) at 1273 K for 6 h.

Oxygen permeation and CH₄ partial oxidation measurements.—An oxygen gas concentration cell of air-Ar, schematically shown in Fig. 1, was used for the simple oxygen permeation measurement. Permeating oxygen from air to Ar was analyzed by using a gas chromatograph. Molten Pyrex glass was used for the gas seal. Since no N₂ in Ar sweep gas was detected by the analysis with gas chromatographs, it was confirmed that the physical gas leakage through the sample and gas seal was negligible.

The same gas concentration cell as shown in Fig. 1 was also used for CH₄ partial oxidation. In the case of CH₄ partial oxidation, Ni and LSC were used as the catalysts for the CH₄ and oxygen side, respectively, at 10 mm and 40 μm diam and thickness. Ni catalyst was obtained by applying the commercial NiO (reagent grade, Wako Pure Chemical) and before reaction, NiO was reduced to Ni by flowing H₂ at 1273 K for 1 h. The outlet gas from the membrane

* Electrochemical Society Active Member.

^z E-mail: isihara@cc.oita-u.ac.jp

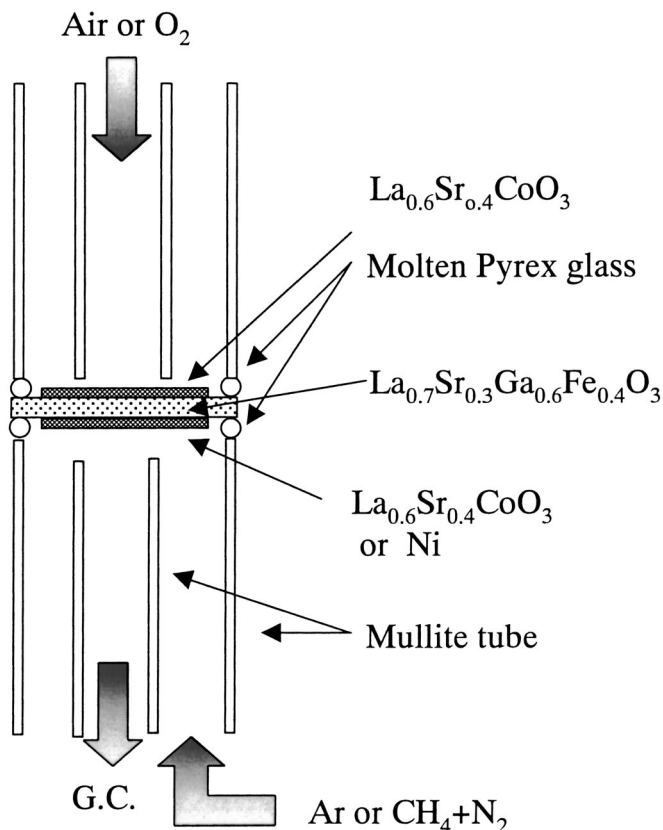


Figure 1. Schematic view of the gas concentration cell used for oxygen permeation as well as CH_4 partial oxidation.

reactor was analyzed by the gas chromatographs with a thermal conductive detector (TCD) with a molecular sieve 5A column.

Electrochemical measurements.—Electrical conductivity was measured with a generally used dc four-probe method in the conventional gas flow cell which is not shown. Partial pressure of oxygen was controlled by using $\text{N}_2\text{-O}_2$, CO-CO_2 , and $\text{H}_2\text{-H}_2\text{O}$ gas mixture and monitored with an oxygen sensor using $\text{Ca}_{0.15}\text{Zr}_{0.85}\text{O}_2$ electrolyte. The transport number of oxide ion was estimated by the ratio of the measured electromotive force (emf) in the $\text{H}_2\text{-O}_2$ cell to that estimated by the Nernst equation. The setup for the $\text{H}_2\text{-O}_2$ cell is quite similar to that shown in Fig. 1. The Wagner polarization method (ion-blocking method) was used for the separation of electronic conductivity from oxide-ion conductivity. The experimental setup for the polarization method is schematically shown in Fig. 2.

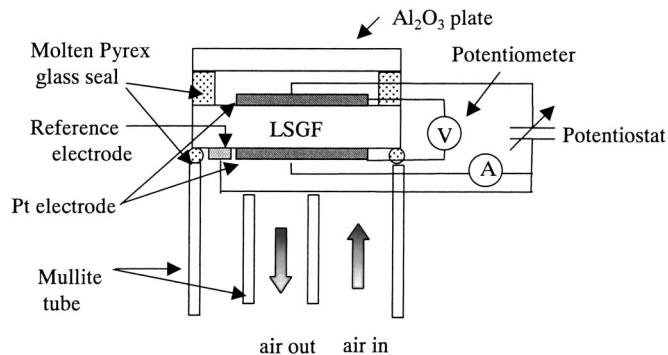


Figure 2. Schematic view of the experimental setup for the polarization method.

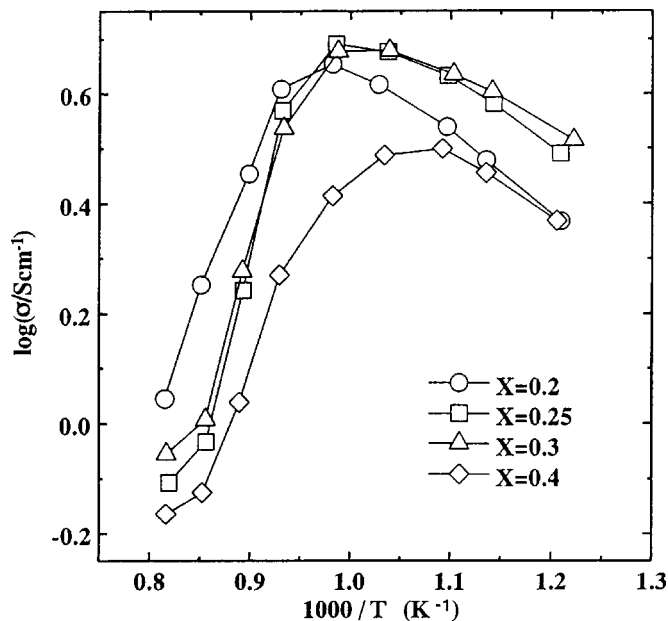


Figure 3. Arrhenius plots of the electrical conductivity of $\text{La}_{1-x}\text{Sr}_x\text{Ga}_{0.6}\text{Fe}_{0.4}\text{O}_3$ in $p_{\text{O}_2} = 10^{-5}$ atm.

An Al_2O_3 dense plate was connected to an Fe-doped LaGaO_3 plate (1 mm in thickness) with a molten Pyrex glass ring and Pt paste (ca. 10 mm diam) attached to the specimens. The reference electrode was attached close to the pumping electrode and the setup was put into air flow stream. A constant potential was applied using a potentiostat (Hokuto Denko, HFBA-501) and current was measured with a digital multimeter (Advantest, R6451). Commercial oxygen was always used as the reference gas. The electrode area for oxygen pumping is much larger than that of the side area of the disks, and the oxygen flux incorporated from the side of the disks does not significantly influence the estimated electronic conductivity.

Results and Discussion

Electrical conducting property of LSGF.—Figure 3 shows Arrhenius plots of the electrical conductivity of $\text{La}_{1-x}\text{Sr}_x\text{Ga}_{0.6}\text{Fe}_{0.4}\text{O}_3$ at $p_{\text{O}_2} = 10^{-5}$ atm. It is seen that all specimens exhibit a high total conductivity in the range 1–10 S/cm. The total conductivity increased with increasing amount of Sr and attained a maximum at $x = 0.3$ at temperature lower than 973 K. Conductivity of all specimens exhibited metal-like temperature dependence at temperatures higher than 973 K, namely, conductivity decreased despite increasing temperature. The generally accepted explanation for this involves the loss of oxygen from the sample at high temperature at the expense of electron holes. This is also related to the thermal reduction of Fe. The conductivity reached a maximum at $x = 0.2$ at temperatures >973 K. In any case, it can be said that $\text{La}_{1-x}\text{Sr}_x\text{Ga}_{0.6}\text{Fe}_{0.4}\text{O}_3$ exhibits a high total conductivity.

Figure 4 shows the electrical conductivity of $\text{La}_{1-x}\text{Sr}_x\text{Ga}_{0.6}\text{Fe}_{0.4}\text{O}_3$ as a function of oxygen partial pressure. In the p_{O_2} range higher than $p_{\text{O}_2} = 10^{-5}$ atm, the electrical conductivity increased with increasing oxygen partial pressure and p_{O_2} dependence of electrical conductivity is almost $p_{\text{O}_2}^{-1/4}$. Consequently, it is clear that the main electronic charge carrier in $\text{La}_{1-x}\text{Sr}_x\text{Ga}_{0.6}\text{Fe}_{0.4}\text{O}_3$ is the electronic hole, which could be assigned to the formation of Fe^{4+} , namely, Fe_{Ga}^+ . The electronic conductivity of $\text{La}_{1-x}\text{Sr}_x\text{Ga}_{0.6}\text{Fe}_{0.4}\text{O}_3$ was almost independent of the oxygen partial pressure in a range of $p_{\text{O}_2} = 10^{-15}$ to 10^{-5} atm. In our previous study on $\text{La}_{0.8}\text{Sr}_{0.2}\text{Ga}_{0.8}\text{Mg}_{0.2-x}\text{Fe}_x\text{O}_3$ (LSGMF),¹⁰ the valence num-

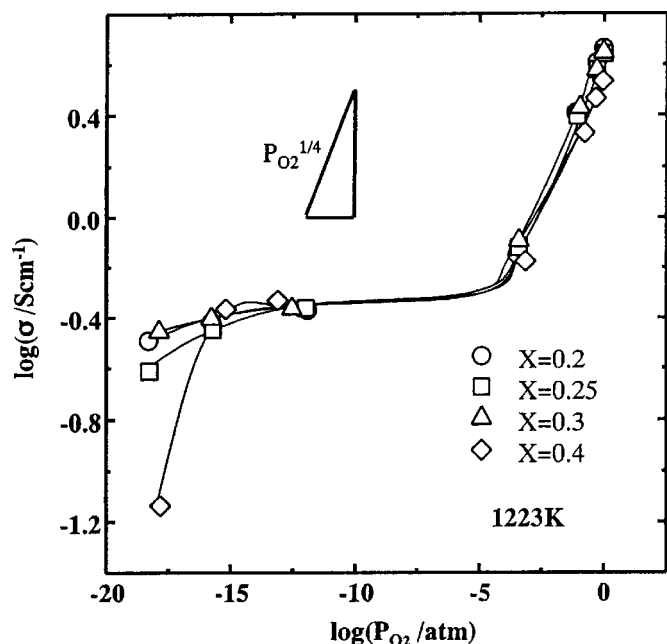
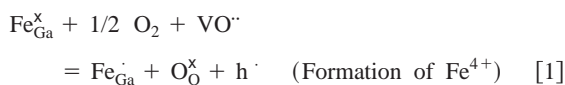
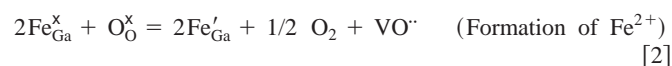


Figure 4. Electrical conductivity of $\text{La}_{1-x}\text{Sr}_x\text{Ga}_{0.6}\text{Fe}_{0.4}\text{O}_3$ as a function of the oxygen partial pressure.

ber of Fe in LSGMF was measured with electron spin resonance (ESR) and it was seen that the ESR signal assigned to Fe^{3+} increased by reducing the sample. Therefore, ESR data suggests that Fe^{3+} is the dominant species and Fe^{4+} forms in the oxidizing atmosphere, expressed as the following equation by Kröger-Vink notation



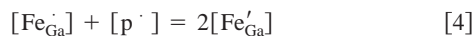
At low p_{O_2} atmosphere, it is considered that Fe^{2+} is formed as the following equation



Therefore, in the intermediate p_{O_2} range, these two equations should be balanced and as following



Since no gaseous oxygen is included in this equation, the electrical conductivity is independent of p_{O_2} , that is shown in Fig. 4. Therefore, amount of Fe^{4+} and hole should be balanced with that of Fe^{2+} as shown in the following equation



in which $[\text{Fe}_{\text{Ga}}^\bullet]$, $[\text{p}^\bullet]$, and $[\text{Fe}_{\text{Ga}}^\bullet]$ represent the amount of Fe^{4+} , electronic hole, and Fe^{2+} , respectively. Although the number of the iron compounds consisting of Fe^{4+} is very limited, it is reported that Fe^{4+} is formed in perovskite-type oxide, SrFeO_3 .¹¹ However, considering the stable valence number, trivalent iron is the dominant species both in O_2 and H_2 atmosphere.

The temperature dependence of the transport number of oxide ion in $\text{La}_{1-x}\text{Sr}_x\text{Ga}_{0.6}\text{Fe}_{0.4}\text{O}_3$, which was estimated by emf in the H_2 - O_2 cell, is shown in Fig. 5. Obviously, emf in H_2 - O_2 cells using $\text{La}_{1-x}\text{Sr}_x\text{Ga}_{0.6}\text{Fe}_{0.4}\text{O}_3$ were almost half those estimated by the Nernst equation, and, furthermore, it changed by changing the p_{O_2} difference across the membrane. Therefore, it can be said that Fe-

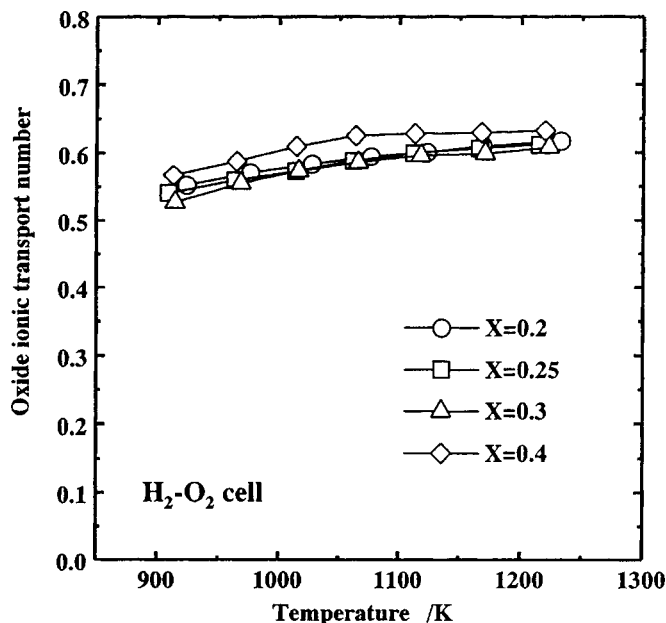


Figure 5. Temperature dependence of the transport number of oxide ions in $\text{La}_{1-x}\text{Sr}_x\text{Ga}_{0.6}\text{Fe}_{0.4}\text{O}_3$.

doped LaGaO_3 exhibits simultaneously high oxide ionic and electronic hole conduction. The largest permeation rate of oxygen is theoretically achieved at 0.5 of the transport number of oxide ion when the total conductivity is the same as shown in Eq. 1. Therefore, Fe-doped LaGaO_3 perovskite-type oxide is suitable as a mixed conductor for the oxygen-permeating membrane. Since the highest electrical conductivity was obtained, LSGF is highly attractive as the mixed electronic-oxide ionic conducting material. Contribution of the electronic charge carrier was further studied by an ion-blocking method.

Electronic conductivity can be separated from that of oxide ion with the Wagner's polarization (ion-blocking) method. In this study, contribution of electronic conductivity to the total conductivity was estimated using the polarization method. Figure 6 shows I_e vs. V curves for LSGF. In the usual case, "S"-shaped curves are observed in these polarization measurements on samples having electronic (n) and hole (p) conduction.^{12,13} However, electronic current I_e increased monotonically with increasing applied potential in the case of LSGF. This suggests that p-type conductivity was always dominant in LSGF and no n-type conductivity was observed at applied

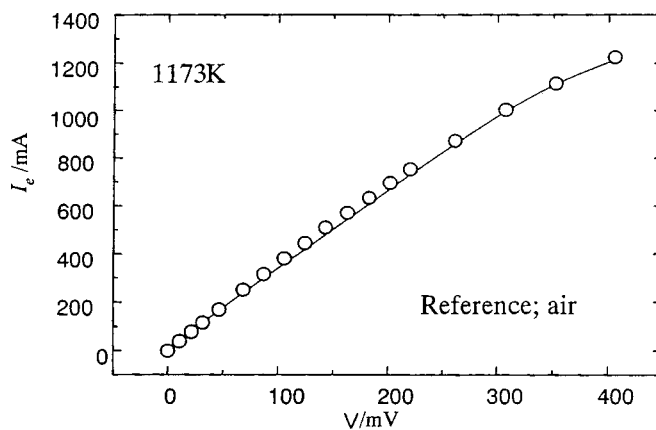


Figure 6. I_e vs. V curves obtained with the ion-blocking technique for LSGF at 1173 K.

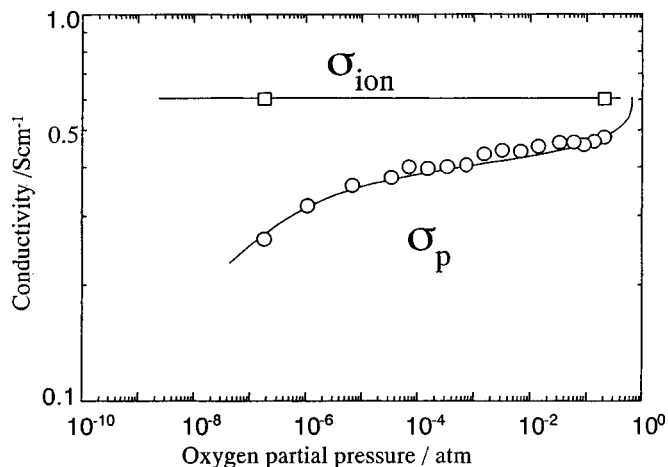


Figure 7. p_{O_2} dependence of hole and oxide-ion conductivity in LSGF at 1172 K.

potentials less than 0.5 V. Electronic hole conductivity can be estimated by the slope of I_e vs. V curves. Also, the applied potential across the sample corresponds to the Nernst emf values across the sample. Since pure oxygen was used for the reference gas, we can estimate the oxygen partial pressure [p_{O_2} (pumping)] in the pumping room from the applied potential and p_{O_2} (Ref.) = 1 atm by using the Nernst equation

$$p_{O_2}(\text{pumping}) = \exp(-4VF/RT) \quad [5]$$

Here, V indicates applied potential and F , R , and T are Faraday constant, gas constant, and temperature, respectively.

p-Type conductivity was estimated based on the polarization measurement and is shown in Fig. 7 as a function of oxygen partial pressure. By subtracting the p-type conductivity from the total conductivity, the oxide-ion conductivity was also estimated, which is also shown in Fig. 7. Since oxide-ion conductivity is independent of the oxygen partial pressure, two points at high and low p_{O_2} were calculated in Fig. 7. It is clear that p-type conductivity in LSGF gradually decreased with decreasing oxygen partial pressure and it became slightly steep at p_{O_2} smaller than 10^{-5} atm. The dependence of p-type conductivity on p_{O_2} is *ca.* 1/50 at $p_{O_2} = 0.21 \times 10^{-5}$ atm. Since the p_{O_2} dependence of total conductivity in Fig. 3 for the corresponding range is *ca.* 1/30, the p_{O_2} dependence of the estimated p-type conductivity is in reasonable agreement. These results also suggest that the main defects in LSGF are Fe_{Ga}^{\bullet} and electronic hole, and the amount of Fe_{Ga}^{\bullet} is balanced with that of V_{O}^{\bullet} . In addition, the estimated transport number of oxide ion by the polarization method was 0.59, which is also in good agreement with that by emf in the H_2 - O_2 gas concentration cell, 0.63. It is also noted that the oxide-ion conductivity in LSGF is extremely high (*ca.* 0.6 S/cm), which is 2.7 times higher than that of oxide-ion conductivity in $La_{0.8}Sr_{0.2}Ga_{0.8}Mg_{0.2}O_3$ (LSGM).

Oxygen-permeating property in LSGF.—Figure 8 shows the temperature dependence of the permeation rate of oxygen through LSGF membrane. In this figure, the oxygen permeation rate through an LSGM membrane at short-circuited condition is also shown as a reference. It is clear that a high oxygen permeation rate was achieved on LSGF membrane at all temperatures. The oxygen permeation rate was attained to be $1.8 \text{ cm}^3 \text{ std}/\text{cm}^2 \text{ min}$ at 1273 K, which is almost three times higher than that of LSGM membrane at the short-circuited condition. The higher oxygen permeation rate of LSGF than that of LSGM suggested that the oxide-ion conductivity

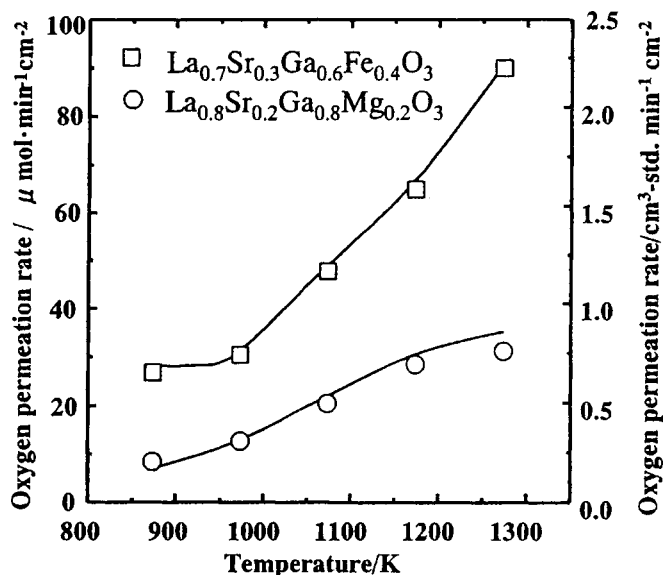


Figure 8. Temperature dependence of the permeation rate of oxygen through LSGF and LSGM membranes (0.5 mm thick). $La_{0.9}Sr_{0.1}Ga_{0.8}Mg_{0.2}O_3$ was short-circuited by using external lead wire.

in LSGF is higher than that of LSGM, since the rate-limiting step for the oxygen permeation through $LaGaO_3$ membrane is the bulk diffusion step. This is because the oxygen permeation rate monotonically increased with decreasing the thickness of membrane in both cases. The oxygen permeation rate of LSGF is 2.3 times higher than that of LSGM. This improvement in oxygen permeation rate is also in good agreement with the improved oxide-ion conductivity shown in Fig. 3. In any case, considering the oxygen-permeating rate of $2.1 \text{ cm}^3 \text{ std}/\text{cm}^2 \text{ min}$ at 1173 K reported for $La_{0.6}Ba_{0.4}Co_{0.8}Fe_{0.2}O_3$,² it can be said that LSGF exhibits large oxygen permeation rate which can be attributed to its fast oxide-ion conductivity.

Figure 9 shows the effects of the thickness of LSGF membrane on the oxygen permeation rate. The oxygen permeation rate through the mixed electronic-oxide ionic conducting membrane is theoretically expressed by the following equation when the bulk diffusion step is the rate-limiting step¹⁴

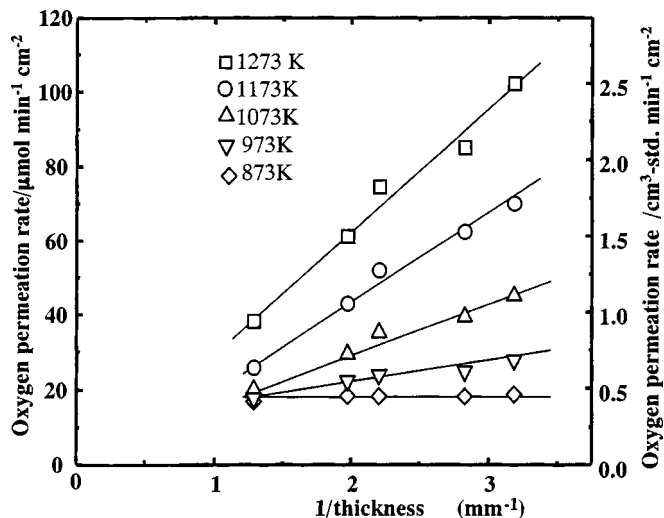


Figure 9. Effects of the thickness of LSGF membrane on the oxygen permeation rate. ($La_{0.6}Sr_{0.4}CoO_3$ was used for the surface catalyst.)

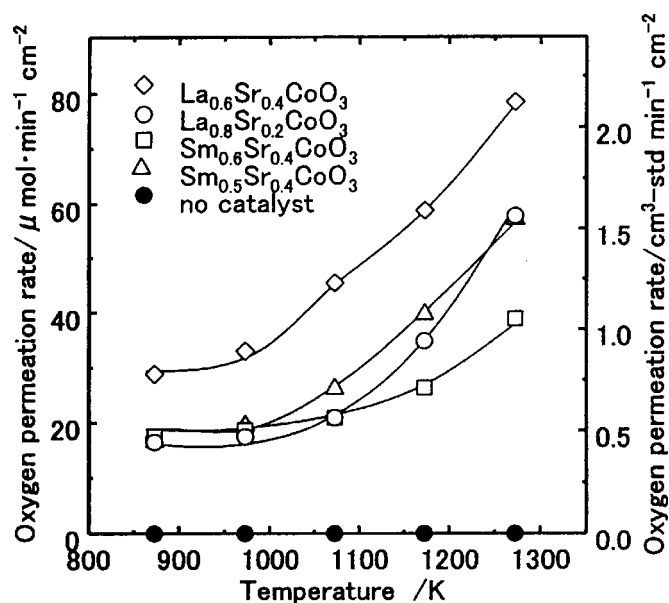


Figure 10. Effects of the surface catalysts on the oxygen permeation rate from air to Ar through LSGF membrane (0.5 mm).

$$J_{O_2} = \frac{RT\sigma_e\sigma_i}{16F^2(\sigma_e + \sigma_i)t} \ln \frac{p_h}{p_l} \quad [6]$$

where J_{O_2} is oxygen permeation rate, t the thickness of membrane, T temperature, R gas constant, p_h and p_l are oxygen partial pressures, F the Faraday constant, and σ_e and σ_i are the electronic and oxide ionic conductivity, respectively. Based on this equation, J_{O_2} is inversely proportional to the thickness of membrane. As shown in Fig. 9, the oxygen permeation rate monotonically increased with decreasing thickness of the membrane, and the oxygen permeating

rate at 1173 K attained a value of $2.5 \text{ cm}^3 \text{ std}/\text{cm}^2 \text{ min}$ when the thickness of the LSGF membrane was 0.3 mm. Therefore, the rate-limiting step for oxygen permeation through LSGF membrane seems to be the bulk diffusion process for the thickness range studied in this paper. Consequently, it is expected that further increase in oxygen permeation rate is obtained by decreasing membrane thickness. However, with decreasing temperature, dependence of oxygen permeation rate on membrane thickness became insignificant. This suggests that the surface reaction rate became slower and was the rate-determining steps with decreasing temperature. Therefore, in order to improve the oxygen permeation rate at 873 K, improvement in catalytic activity is required.

Effects of the surface catalysts on the oxygen permeation rate in LSGF membrane were further studied and the results are shown in Fig. 10. The oxygen permeation rate was strongly dependent on the surface catalyst. Since almost no oxygen permeation was observed through LSGF membrane when no catalyst was applied as shown in Fig. 10, surface catalyst is essential for obtaining the high oxygen permeation rate. This suggests that the surface activity of LSGF to oxygen dissociation reaction is low; however, oxide ion diffusivity in bulk is high. Consequently, the oxygen permeation through LSGF membrane is strongly influenced by surface catalyst, and it was seen that the oxygen permeation from air to Ar at 1273 K increased in the following order. $\text{La}_{0.6}\text{Sr}_{0.4}\text{CoO}_3 > \text{La}_{0.8}\text{Sr}_{0.2}\text{CoO}_3 \approx \text{Sm}_{0.5}\text{Sr}_{0.5}\text{CoO}_3 \gg \text{Sm}_{0.6}\text{Sr}_{0.4}\text{CoO}_3$ as the surface catalyst. It was reported that $\text{Sm}_{0.5}\text{Sr}_{0.5}\text{CoO}_3$ exhibits the highest activity to the cathodic reaction of solid oxide fuel cells (SOFCs) using LaGaO_3 -based electrolyte at intermediate temperature.^{15,16} Therefore, it is considered that SmCoO_3 is highly active for the oxygen dissociation reaction. However, $\text{La}_{0.6}\text{Sr}_{0.4}\text{CoO}_3$, which is not so highly active to the cathodic reaction of SOFC, exhibited the highest activity for oxygen permeation. Therefore, it seems likely that the surface reaction steps contained in the oxygen permeation are different from those in the cathode of the fuel cell. In any case, it was seen that $\text{La}_{0.6}\text{Sr}_{0.4}\text{CoO}_3$ is the preferable surface catalyst for the LSGF oxygen-permeating membrane among the examined oxides.

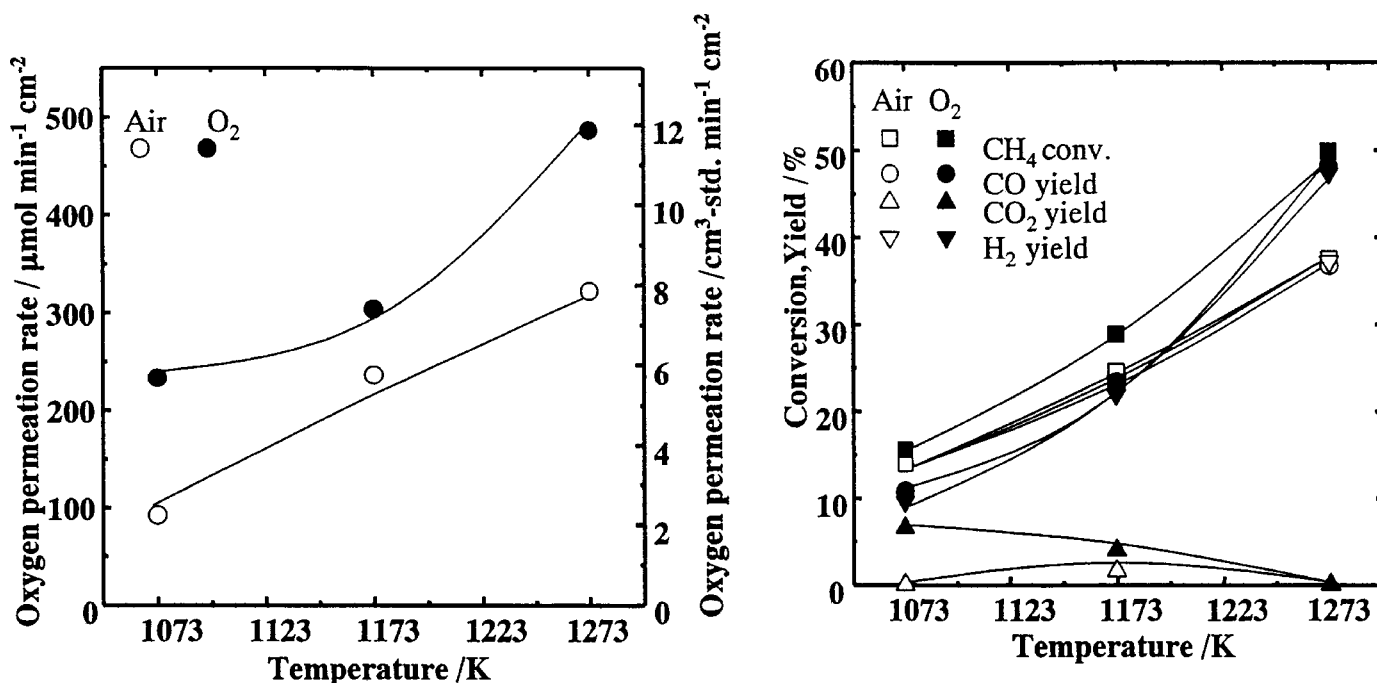


Figure 11. Temperature dependence of oxygen permeation rate, CH_4 conversion, and yield of CO and H_2 . ($\text{La}_{0.6}\text{Sr}_{0.4}\text{CoO}_3$ and Ni were used for air and CH_4 side catalysts, respectively.)

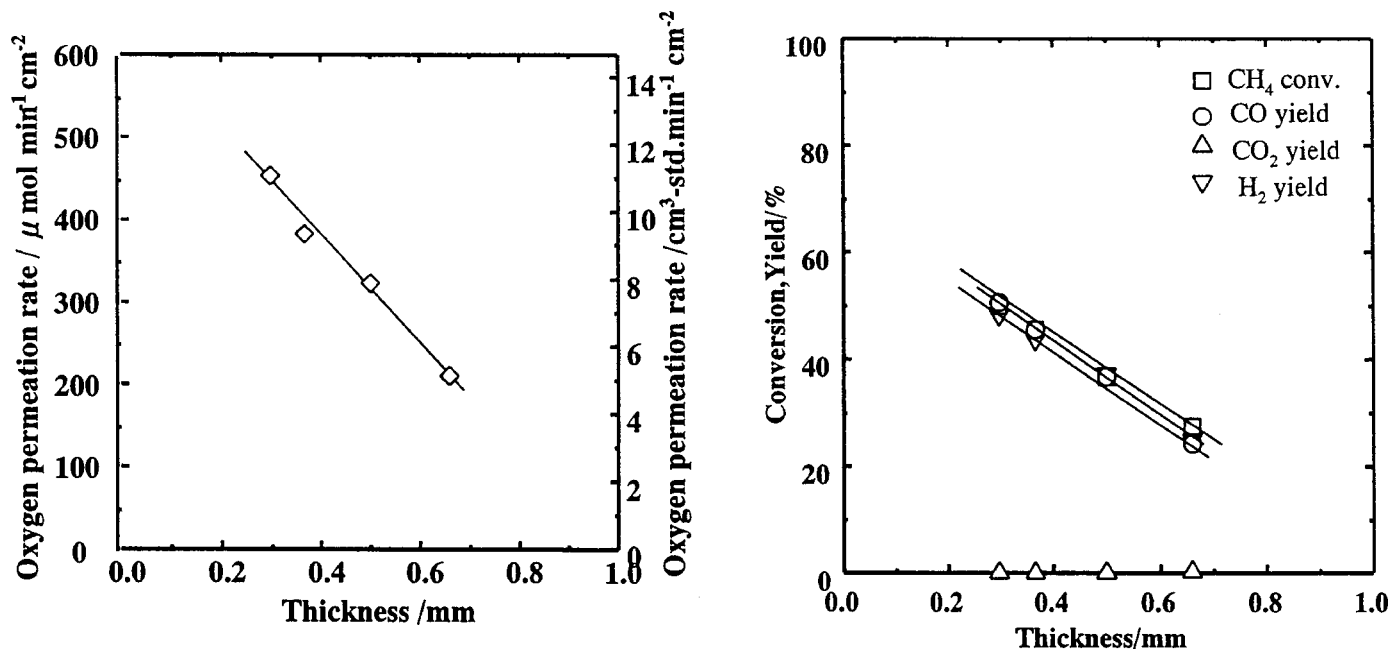


Figure 12. Oxygen permeation rate and the product yield in CH_4 partial oxidation as a function of membrane thickness at 1273 K.

The oxygen-permeating property of LSGF under CH_4 partial oxidation.—Application of LSGF to the oxygen-permeating membrane for CH_4 partial oxidation was further studied. Figure 11 shows the temperature dependence of oxygen permeation rate, CH_4 conversion, and yield of CO and H_2 . It is clear that the oxygen permeation rate increased drastically by changing Ar to CH_4 in the permeation side. This increase in oxygen permeation is predicted from Eq. 6 because the p_{O_2} gradient becomes steeper. The permeation rate attained a value of ca. $8 \text{ cm}^3 \text{ std/min cm}^2$ at 1273 K when the thickness of the electrolyte was 0.5 mm. CH_4 conversion of 40% and yield of CO and H_2 at the same value to CH_4 conversion were also obtained at 1273 K. Because the yield of CO and H_2 were almost the same as that of CH_4 conversion and CO_2 formation was negligibly small, it is obvious that the CH_4 partial oxidation dominantly proceeds in the membrane reactor using LSGF as the oxygen-permeating membrane.

Effects of oxygen partial pressure in oxidant on the permeation rate through LSGF membrane under the CH_4 partial oxidation were further studied and the results are compared in Fig. 11. It is reasonable that oxygen permeation rate further increased by changing from air to oxygen at all temperatures examined. This suggests that the rate-limiting step of the oxygen permeation under the CH_4 partial oxidation is still a bulk diffusion process. The amount of oxygen permeation was as high as 12 and $6 \text{ cm}^3 \text{ std/min cm}^2$ at 1273 and 1073 K, respectively, when the thickness of the membrane is 0.5 mm. CH_4 conversion was also improved by changing air to oxygen. However, formation of CO_2 was observed and it became significant with decreasing reaction temperature when oxygen was used as oxidant. This suggests that the surface activity of the Ni catalyst used for the partial oxidation of CH_4 was not high enough, and the amount of permeating oxygen became excess when pure oxygen was used as a source of oxygen. Therefore, further increase in the yield of CO and H_2 can be achieved (if the activity of Ni can be improved by improving dispersion). It is also noted that the pressurizing air also gives the same positive effects on the oxygen permeation rate. Even at 873 K, the rate-determining step for oxygen permeation seems to be the bulk diffusion, and so it is expected that the oxygen permeation rate can be further improved by decreasing

the thickness of the LSGF membrane or increasing the p_{O_2} gradient across the membrane.

Figure 12 shows the oxygen permeation rate and the product yield in CH_4 partial oxidation as a function of membrane thickness at 1273 K. It is clear that the oxygen permeation rate monotonically increased with decreasing the thickness of the LSGF membrane. These results also suggested that the rate-limiting step for the CH_4 partial oxidation is a bulk diffusion step even for 0.3 mm thick membrane. The permeation rate from air to CH_4 was $12 \text{ cm}^3 \text{ std/min cm}^2$ at 1273 K as shown in Fig. 12. In accordance with the increase in the amount of permeating oxygen, CH_4 conversion as well as yield of CO and H_2 also increased monotonically. Since the amount of carbon was almost balanced before and after the reaction, no carbon seems to form on Ni catalyst. Absence of carbon formation on Ni catalyst was also confirmed by visual examination after partial oxidation reaction. H_2/CO ratio was always close to two. Consequently, it seems that no carbon was deposited during CH_4 partial oxidation in the LSGF membrane reactor and the CH_4 partial oxidation into CO/ H_2 gas was the dominant reaction. Therefore, the CH_4 partial oxidation process combined with the oxygen separation membrane using mixed oxide ion conductor is highly attractive for the conversion of CH_4 into liquid fuels, because the size of the reactor is small and the process is also simple.

Figure 13 shows the X-ray diffraction (XRD) patterns before and after CH_4 partial oxidation for 12 h. It was seen that no significant difference was observed on the XRD patterns of the LSGF membrane before and after the CH_4 partial oxidation reaction. Therefore, the LSGF membrane has enough stability against reduction and oxidation. SEM observation also confirmed that there is no crack observed on the surface of the membrane. Absence of crack formation during CH_4 partial oxidation is also confirmed by no N_2 leakage observed in the product stream. Consequently, it can be concluded that LSGF has good chemical stability, which is enough for the oxygen-permeating membrane for the CH_4 partial oxidation.

Conclusion

Although mixed oxide-ion conductivity in LaGaO_3 -based oxide has not been studied extensively, it was found that Fe-doped,

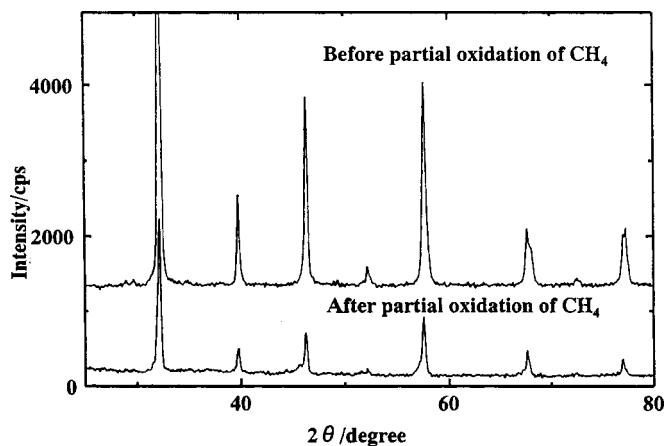


Figure 13. XRD patterns of LSGF before and after CH_4 partial oxidation at 1273 K.

LaGaO_3 -based oxide exhibited high mixed electronic hole and oxide ion conductivity. Therefore, a high oxygen-permeating rate was achieved on LSGF membranes. The ion-blocking method shows the main charge carrier in LSGF is hole and oxide ion. It is also noted that the oxide ion conductivity in LSGF is extremely large (0.6 S cm^{-1} at 1173 K). Therefore, $\text{La}_{0.7}\text{Sr}_{0.3}\text{Ga}_{0.6}\text{Fe}_{0.4}\text{O}_3$ is highly attractive, not only as the oxygen-permeating membrane but also as the fast oxide ion conductor. LaGaO_3 -based oxide has a high stability against reduction, and $\text{La}_{0.7}\text{Sr}_{0.3}\text{Ga}_{0.6}\text{Fe}_{0.4}\text{O}_3$ exhibits a large oxygen permeation rate under CH_4 partial oxidation condition. An oxygen-permeating ceramic membrane for the partial oxidation of CH_4 is one of the most desirable applications of a mixed conductor. Consequently, it can be concluded that LSGF is highly attractive as a material for oxygen-permeating membranes.

Acknowledgments

The authors acknowledge financial support from a Grant-in-Aid for Science Promotion from the Ministry of Education, Culture, Sports, Science, and Technology of Japan (no. 11102006 and 13355032). Financial support from NEDO is also appreciated.

Oita University assisted in meeting the publication costs of this article.

References

1. S. Pei, M. S. Kleefisch, T. P. Kobylinski, J. Faber, C. A. Udovich, V. Zhang-McCoy, B. Dabroaski, U. Balachandran, R. L. Mieville, and R. B. Poeppel, *Catal. Lett.*, **30**, 201 (1995).
2. C. Y. Tsai, A. G. Dixon, Y. H. Ma, W. R. Moser, and M. R. Pascucci, *J. Am. Ceram. Soc.*, **81**, 1437 (1998).
3. H. Kusaba, G. Sakai, N. Miura, and N. Yamazoe, *Electrochemistry*, **68**, 409 (2000).
4. Y. Teraoka, T. Nobunaga, and N. Yamazoe, *Chem. Lett.*, **1990**, 1.
5. B. Ma, U. Balachandran, J.-H. Park, and C. U. Segre, *Solid State Ionics*, **83**, 65 (1996).
6. U. Balachandran, J. T. Dusek, S. M. Sweeney, R. B. Poeppel, R. L. Mieville, P. S. Maiya, M. S. Kleefisch, S. Pei, T. P. Kobylinski, and C. A. Udovich, *Am. Ceram. Soc. Bull.*, **74**, 71 (1995).
7. H. Arikawa, T. Yamada, T. Ishihara, H. Nishiguchi, and Y. Takita, *Chem. Lett.*, **1999**, 1257.
8. T. Ishihara, T. Yamada, H. Arikawa, H. Nishiguchi, and Y. Takita, *Solid State Ionics*, **135**, 631 (2000).
9. Y. Tsuruta, T. Todaka, H. Nishiguchi, T. Ishihara, and Y. Takita, *Electrochem. Solid-State Lett.*, **4**, E13 (2001).
10. T. Ishihara, T. Shibayama, M. Honda, H. Nishiguchi, and Y. Takita, *J. Electrochem. Soc.*, **147**, 1337 (2000).
11. T. C. Gibb, *J. Chem. Soc. Dalton Trans.*, **1986**, 1447.
12. R. T. Baker, B. Gharbage, and F. M. B. Marques, *J. Electrochem. Soc.*, **144**, 3130 (1997).
13. J. H. Kim and H. I. Yoo, *Solid State Ionics*, **140**, 105 (2001).
14. N. Itoh, T. Kato, K. Uchida, and K. Haraya, *J. Membr. Sci.*, **92**, 239 (1994).
15. T. Ishihara, M. Honda, T. Shibayama, H. Minami, H. Nishiguchi, and Y. Takita, *J. Electrochem. Soc.*, **145**, 3177 (1998).
16. H. Y. Tu, Y. Takeda, N. Imanishi, and O. Yamamoto, *Solid State Ionics*, **100**, 283 (1997).